# Supplementary Materials for "Study of quasi-particle dynamics using the optical pulse response of a superconducting resonator"

J. Hu[1], Q. He[2], F. Yu[2], Y. Chen[1], M. Dai[2], H. Guan[1], P. Ouyang[2], J. Han[2], C. Liu[1], X. Dai[1], Z. Mai[1], X. Liu[1], M. Zhang[1], L. F. Wei[2], M. R. Vissers[3], J. Gao[3], and Y. Wang[1*]

*1) Quantum Optoelectronics Laboratory,*

*School of Physical Science and Technology,*

*Southwest Jiaotong University, Chengdu, Sichuan 610031, China*

*2) Information Quantum Technology Laboratory,*

*School of Information Science and Technology,*

*Southwest Jiaotong University, Chengdu, 610031, China*

*3) National Institute of Standards and Technology, Boulder, CO 80305, USA*

(Dated: June 28, 2021)

* Electronic mail: qubit@swjtu.edu.cn

### A. Equivalent Resonance Circuit

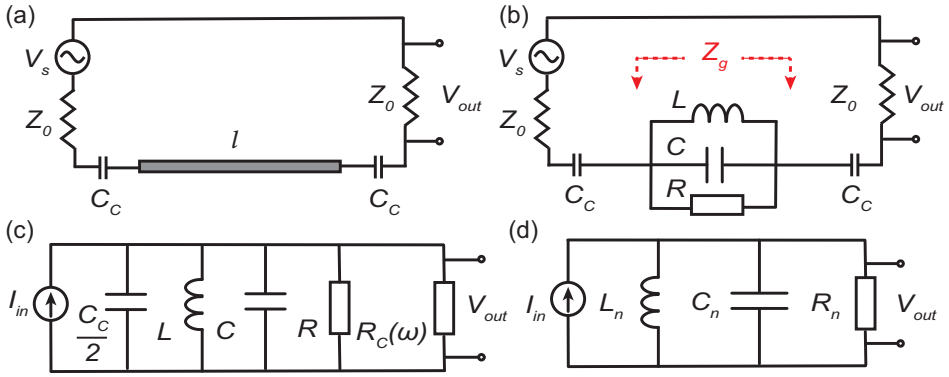


FIG. S1: (a) Open circuit half-wavelength CPW with coupling capacitance $C_c$ to input and output ports. (b) Near the fundamental resonance frequency, the CPW behaves as a parallel $LCR$ circuit. (c) Using NORTON's equivalence theorem, the original circuit behaves as a CPW resonator in parallel with $R_c(\omega)$ and $C_c/2$. (d) For the $n$-th resonance modes, the original circuit can be modelled as a lumped-element $L_nC_nR_n$ parallel circuit with a current source $I_{in}$.

According to the transmission line theory, the input impedance of an open-circuited CPW (FIG. S1(a)) with length $l$ is

$$Z_{in} = Z_0 \coth(\alpha + j\beta) = Z_0 \frac{1 + j\tan(\beta l)\tanh(\alpha l)}{\tanh(\alpha l) + j\tan(\beta l)} \tag{S1}$$

where $\alpha + j\beta$ is the complex propagation constant and $Z_0 = \sqrt{\tilde{L}/\tilde{C}}$ is the characteristic impedance of the CPW (matched with the input and load impedance). Here $\tilde{L}$ and $\tilde{C}$ are distributed inductance and capacitance of the CPW per unit length respectively.

Near the half-wave resonance condition, we can write $\beta l = \pi(1 + \Delta\omega/\omega_0)$, where $\Delta\omega = \omega - \omega_0$ and $\omega_0 = \pi/(l\sqrt{\tilde{L}\tilde{C}})$ is the fundamental resonance frequency. For a CPW with small loss $\alpha l << 1$ and at a frequency close to the resonance frequency, we have $\tanh(\alpha l) \approx \alpha l$ and $\tan \beta l \approx \pi\Delta\omega/\omega_0$, then Eqn. (S1) can be approximated to:

$$Z_{in} = \frac{Z_0}{\alpha l + j\pi\Delta\omega/\omega_0} \tag{S2}$$

Eqn. (S2) takes the same form as a parallel $LCR$ resonance circuit (FIG. S1(b)) with input impedance:

$$Z_{in} = \frac{R}{1 + 2j\Delta\omega RC} = \frac{R}{1 + 2jQ\Delta\omega/\omega_0} \tag{S3}$$

By comparing Eqn. (S2) and Eqn. (S3), one can obtain the relations between lumped-element $LCR$ parameters and the distributed circuit parameters:

$$L = \frac{2l}{\pi^2}\tilde{L} \quad C = \frac{l}{2}\tilde{C} \quad R = \frac{Z_0}{\alpha l} \tag{S4}$$

$L$ and $C$ sets the fundamental resonance frequency at $\omega_0 = 1/\sqrt{LC}$, and the internal quality factor (due to internal dissipation) is given by $Q = \omega_0 RC$. The Norton equivalent impedance seen from the two ends of the CPW is:

$$Z_g = 2(Z_0 + \frac{1}{j\omega C_c}) \tag{S5}$$

For weak coupling condition ($\omega C_c Z_0 \ll 1$), the Norton admittance is:

$$Y_g = \frac{1}{Z_g} \approx \frac{j\omega C_c}{2} + \frac{1}{R_c(\omega)} \tag{S6}$$

where

$$R_c(\omega) = \frac{2}{Z_0(\omega C_c)^2} \tag{S7}$$

which relates to the coupling quality factor by $Q_c = \omega R_c(\omega)(C + C_c/2) \approx \omega R_c(\omega)C$. Eqn. (S6) indicates that the original circuit can be modelled as a CPW resonator in parallel with a small capacitance $C_c/2$ and a frequency-dependent resistance $R_c(\omega)$, which is shown in FIG. S1(c).

The above derivation for the fundamental resonance frequency can be generalized to all resonance modes. Around the $n$-th resonance frequencies $\omega_n = n\omega_0$ ($n = 1, 2, 3, ...$), we have $\beta l = n\pi(1 + \Delta\omega/\omega_0)$ and $\tan \beta l \approx n\pi\Delta\omega/\omega_0$. Then it can be derived that the equivalent lumped-element parameters are given by:

$$L_n = \frac{1}{n^2}L \quad C_n = C + \frac{C_c}{2} \quad R_{cn} = \frac{1}{n^2}R_c \quad Q_{cn} = \frac{1}{n}Q_c \tag{S8}$$

$L_n$ and $C_n$ sets the $n$-th resonance frequency at $\omega_n = 1/\sqrt{L_n C_n} = n\omega_0$. $R_{cn}$ and $R$ (internal resistance) in parallel result in a total equivalent resistance $R_n$ and a corresponding total quality factor $Q_n = \omega_n R_n C_n$. These parameters satisfy the relations $1/R_n = 1/R + 1/R_{cn}$ and $1/Q_n = 1/Q + 1/Q_{cn}$. The equivalent lumped-element circuit for $n$-th resonance mode is shown in FIG. S1(d).

**B. Variable Inductance Model**

To simulate the time-dependent change of the kinetic inductance due to quasi-particle generation and recombination, we develop a variable inductance model based on the Simulink

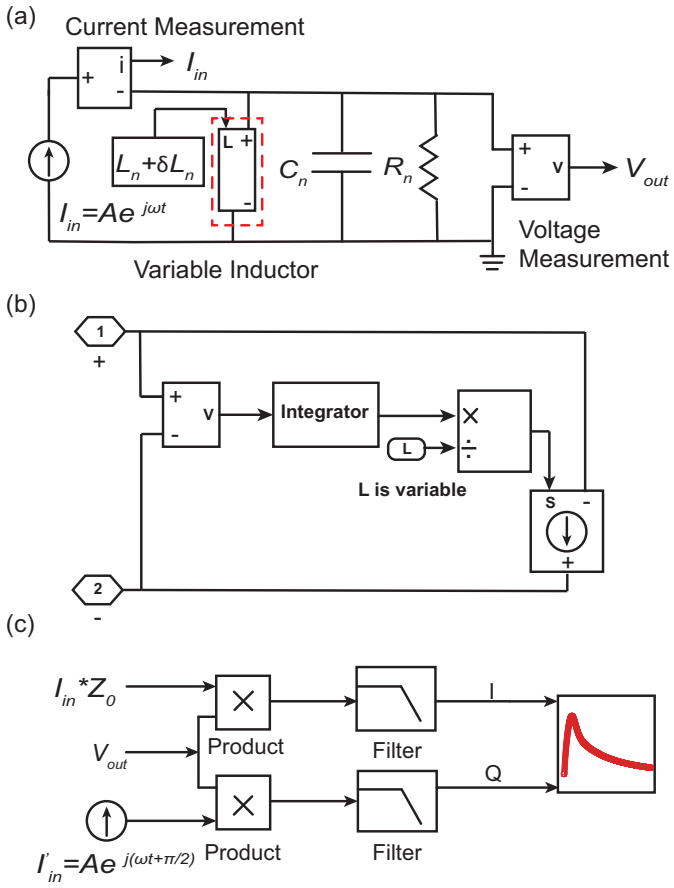


FIG. S2: (a) The simulated resonance circuit with a variable inductance. (b) The inner circuit of the variable inductance block. (c) I/Q mixing and demodulation.

of MATLAB [1], which can serve as a general and quantitative approach to analyze the optical pulse response of a resonator. FIG. S2(a) shows the simulated resonance circuit with a variable inductance block which follows the Faraday's law. FIG. S2(b) shows the inner circuit of this variable inductance block and the current is defined to flow from the positive terminal to the negative terminal. The voltage across the variable inductor is $V(t) = L(t)\mathrm{d}(I(t))/\mathrm{d}t + I(t)\mathrm{d}(L(t))/\mathrm{d}t$ and the instantaneous current through the inductor is $I(t) = \int V(t)\mathrm{d}t/L(t)$.

In simulation, we set the values of inductance $L_n$ and resistance $R_n$ to match the resonance frequency and total quality factor in experiments. The capacitance $C_n$ is determined by Sonnet simulation. We input a microwave current with constant amplitude at a frequency on resonance with the $LCR$ circuit, and the time-dependent voltage can be measured at the output. As shown in FIG. S2(c), the input and output voltage signals are mixed and filtered

by a low pass filter to give the demodulated signal in the complex plane (I/Q data).

Here we take the case of fundamental resonance ($n = 1$) as an example to demonstrate the validity of our simulation model. From Sonnet simulation, we can obtain the distributed capacitance of the designed half-wavelength CPW $\tilde{C} = 1.507 \times 10^{-10}$ F/m, which gives the equivalent capacitance $C_1 = 4.4788$ pF (according to Eqn.(S8)). The equivalent inductance $L_1 = 6.174576$ nH and resistance $R_1 = 1.418358 \times 10^6$ Ohm set the resonance frequency $f_1 = 0.957052$ GHz and the total quality factor $Q_1 = 38.2 \times 10^3$, which are in consistent with experiments. We first sweep 201 frequency points centered at $f_1$ with an appropriate frequency span $= 10f_1/Q_1$. The simulated resonance circle in the complex plane is shown in FIG. S3(a). By fitting this resonance circle, we can extract the phase-frequency relation, as shown in FIG. S3(b).

Then we simulate the optical pulse response at the resonance frequency $f_1$. We apply a sudden and small change $\delta L_1(t)$ in the inductance, i.e., $L_1(t) = L_1 + \delta L_1(t)$ ($\delta L_1(t) \ll L_1$). As shown in FIG. S3(c) (red curve), $\delta L_1(t)$ has a linear slope for the first 200 ns and reaches its maximum $\delta L_1(t)/L_1 = 6.4 \times 10^{-7}$ at $t = 200$ ns. After that, $\delta L_1(t)$ decays exponentially as $e^{-t/\tau}$, where $\tau = 40$ $\mu$s. The input variable $\delta L_1(t)$ will lead to a dynamical phase shift at the output, which is then converted to a frequency shift according to the phase-frequency relation (FIG. S3(b)). The simulated relative resonance frequency shift $\delta f_1(t)/f_1$ is shown in FIG. S3(d) (red curve). One can see that the frequency shift peaks at $t \approx 20$ $\mu$s, which is the response time of the resonance circuit. The maximum of $\delta f_1(t)/f_1$ is smaller than the maximum of $\delta L_1(t)/L_1$. The response curve also has a slower falling edge compared to the input inductance variations. These features are all observed in experiments.

Gao's thesis [2] provides a perturbation analysis on the dynamic response of the resonator. Assume we have a small and slow time-dependent inductance variation, which is a narrow-banded signal with Fourier transform $\delta L(t) = \int \delta L(\tilde{f}) e^{2\pi \tilde{f} t} \mathrm{d}\tilde{f}$. It can be derived that when the resonator is driven on resonance $f = f_n$, the Fourier transform of the time-dependent transmission variation $\delta S_{21}(t)|_{f=f_n}$ is $\delta S_{21}(\tilde{f})$, which is proportional to $\delta L(\tilde{f})/(1+j2Q\tilde{f}/f_n)$, indicating that the resonator acts as a low-pass filter with a bandwidth equal to the resonator's bandwidth $f_n/2Q$. Then in principle the instant transmission variation $\delta S_{21}(t)$ can be obtained by integrating the inverse Fourier transform $\int \mathrm{d}\tilde{f} e^{2\pi \tilde{f} t} \delta L(\tilde{f})/(1 + j2Q\tilde{f}/f_n)$. As shown in FIG. S3(d), the theoretical response (blue dotted curve) based on perturbation analysis is identical to the simulated response, demonstrating the validity of both the pertur-

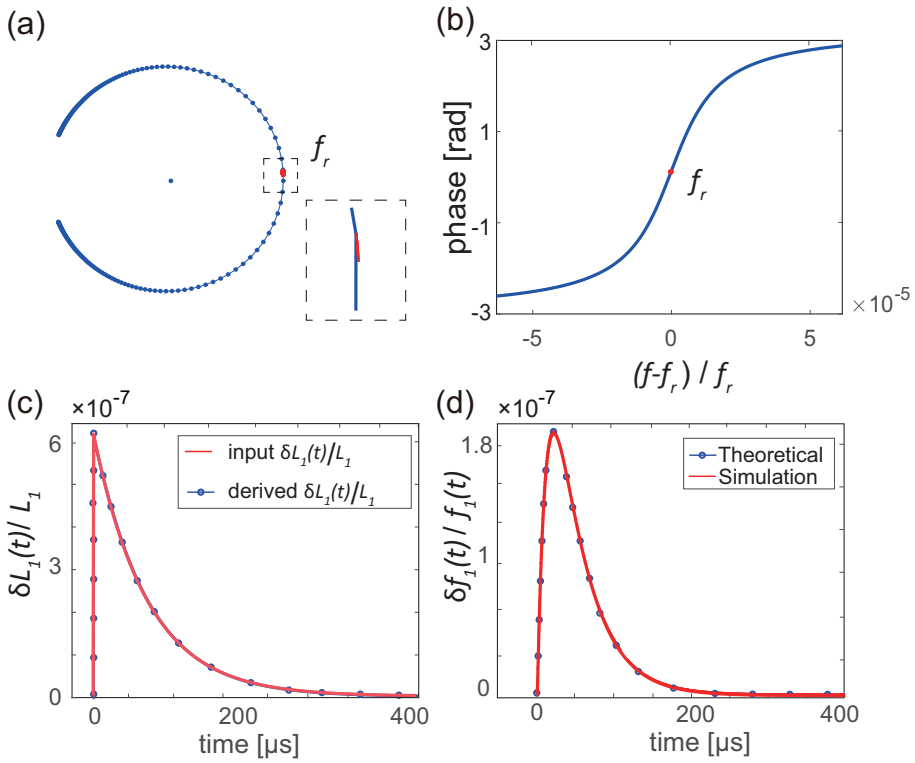


FIG. S3: (a) The simulated resonance circle (blue dotted curve) in the complex plane. The red curve (see zoom-in image in the inset) shows the pulse response due to a small inductance variation. (b) The extracted phase-frequency relation from the simulated resonance circle. (c) The input variable $\delta L_1(t)/L_1$ (red curve), and the derived $\delta L_1(t)/L_1$ (blue dots) from the frequency response using an iterative method. The agreement between these two curves demonstrate that our iterative method is effective to retrieve inductance variation in the time domain. (d) The simulated frequency response (red curve) and the theoretical response (blue dots) based on perturbation analysis, showing perfect agreements.

bation analysis and our simulation model. Note that, the perturbation analysis only holds for small inductance variation ($\delta L(t) \ll L$) and the frequency of the inductance variation should be much smaller then the microwave signal frequency. Besides, a long time series of signal is needed in order to correctly implement the Fourier transform. However, our numerical simulation model is not limited to these conditions and therefore can be used in wider applications.

From the frequency response, one can use an iterative method to retrieve the input time-dependent inductance variations. We first try the falling stage of the target frequency

response $\delta f_1(t)/f_1$ as the initial solution for the shape of inductance variation ($\delta L_1(t)/L_1$). We adjust the inductance variation maximum so that the magnitude of the simulated frequency response is roughly consistent with the target frequency response. Then we gradually correct the shape of the inductance variation based on the difference between the simulated result and the target frequency response. For each correction, the response time and decay profile of simulated response has a better match with the target frequency response. In the mean time, the maximum of $\delta L_1(t)/L_1$ also needs to be slightly adjusted. After a few iterations, we can get a simulated response which is almost identical to the target frequency response. As shown in FIG. S3(c), the retrieved inductance variation (blue dots) shows remarkable agreements with the original inductance variation (red curve), with a small difference in the magnitude less than 0.5%. The above results demonstrate the validity of both the simulation model and iterative method, which is used in our paper to retrieve (estimate) the real inductance variation from the experimental resonator response.

### C. Gaussian diffusion model

We now consider a simple one-dimensional model which can describe both effects of quasi-particle recombination (relaxation) and diffusion. The quasi-particle density is a function of position and time, satisfying the following equation:

$$\frac{\mathrm{d}n(x,t)}{\mathrm{d}t} + \frac{n(x,t)}{\tau} = D\frac{\mathrm{d}^2 n(x,t)}{\mathrm{d}x^2} \tag{S9}$$

where $D$ is the quasi-particle diffusion constant in the superconductor and $\tau$ is a constant quasi-particle lifetime. For a Gaussian distribution of quasi-particle with initial width $\sigma_0$ at $t = 0$ and centered at $x = 0$, the solution of Eqn. (S9) can be easily obtained:

$$n(x,t) = n_0 e^{-t/\tau}\frac{\sigma_0}{\sigma(t)}e^{-\frac{x^2}{2\sigma^2(t)}} \tag{S10}$$

where $n_0$ is the quasi-particle density at $x = 0$ and $t = 0$, and the quasi-particle distribution width at time $t$ is given by $\sigma^2(t) = \sigma_0^2 + 2Dt$. However, the relaxation of quasi-particle might be related to the quasi-particle density with a more complicated form than Eqn. (S9). For example, higher order terms of $n(x,t)$ (e.g., $n^2(x,t)$) can be included in Eqn. (S9), resulting in a more complicated relaxation process which is hard to be expressed analytically. In our paper, we assume the quasi-particle density can still be written in the form:

$$n(x,t) = n_0 f(t)\frac{\sigma_0}{\sigma(t)}e^{-\frac{x^2}{2\sigma^2(t)}} \tag{S11}$$

where $f(t)$ is a time-dependent function but does not have to be an exponential decay. Based on this model, we can calculate the ratio of $\delta L_n(t)/L_n(t)$ between only one pair of odd and even resonance modes to estimate the QP diffusion parameters (diffusion constants $D$ and initial width $\sigma_0$). The results are given in TABLE S1:

| Ratio | 50 mK | | | 350 mK | | |
|---|---|---|---|---|---|---|
| | $D$ | $D^*$ | $\sigma_0$ | $D$ | $D^*$ | $\sigma_0$ |
| Res.2/1 | 148.5 | 140.3 | 1.34 | 179.7 | 182.9 | 1.58 |
| Res.2/3 | 163.7 | 151.8 | 1.67 | 250.7 | 253.7 | 1.76 |
| Res.2/5 | 158.8 | 148.8 | 1.69 | 227.6 | 228.0 | 1.73 |
| Res.4/1 | 83.2 | 80.0 | 1.02 | 147.6 | 147.2 | 1.15 |
| Res.4/3 | 106.9 | 102.8 | 1.29 | 237.6 | 236.4 | 1.30 |
| Res.4/6 | 108.1 | 103.7 | 1.33 | 220.2 | 218.1 | 1.31 |
| Res.6/1 | 47.6 | 43.4 | 0.85 | 85.1 | 78.1 | 0.97 |
| Res.6/3 | 73.4 | 66.3 | 1.10 | 174.8 | 162.4 | 1.10 |
| Res.6/5 | 78.2 | 66.3 | 1.14 | 174.8 | 162.4 | 1.12 |
| Average | 103.1 | 97.7 | 1.27 | 187.2 | 184.7 | 1.33 |

$\star$ The units of $D$ ($D^*$) and $\sigma_0$ are $\mathrm{cm}^2/\mathrm{s}$ and mm respectively.

TABLE S1: Estimated diffusion constant $D$ and initial QP width $\sigma_0$. For 50 mK, $D$ ($D^*$) is obtained by fitting data from 50 $\mu$s to 200 $\mu$s (100 $\mu$s to 200 $\mu$s). For 350 mK, $D$ ($D^*$) is obtained by fitting data from 30 $\mu$s to 150 $\mu$s (80 $\mu$s to 150 $\mu$s). The QPs relax faster at 350 mK than 50 mK, so we set 200 $\mu$s (150 $\mu$s) as the cut-off time for data at 50 mK (350 mK).


[1] https://www.mathworks.com/help/physmod/sps/ug/variable-inductance-modeling.html

[2] J. Gao, Ph.D. thesis, Caltech, 2008.

[3] J. Zmuidzinas, Annual Review of Condensed Matter Physics **3**, 169 (2012).